Photoinduced Charge Carrier Generation and Decay in Sequentially Deposited Polymer/Fullerene Layers: Bulk Heterojunction vs. Planar Interface

ARTICLE *in* THE JOURNAL OF PHYSICAL CHEMISTRY C · APRIL 2012

Impact Factor: 4.77 · DOI: 10.1021/jp212390p

6 AUTHORS, INCLUDING:

Alexandre Nardes
National Renewable Energy Laboratory
38 PUBLICATIONS **1,225** CITATIONS
SEE PROFILE

Scott R. Hammond
National Renewable Energy Laboratory
21 PUBLICATIONS **248** CITATIONS
SEE PROFILE

Nikos Kopidakis
National Renewable Energy Laboratory, Gol…
117 PUBLICATIONS **5,563** CITATIONS
SEE PROFILE

THE JOURNAL OF PHYSICAL CHEMISTRY C

Article

pubs.acs.org/JPCC

Photoinduced Charge Carrier Generation and Decay in Sequentially Deposited Polymer/Fullerene Layers: Bulk Heterojunction vs Planar Interface

Alexandre M. Nardes,[†] Alexander L. Ayzner,[‡,§] Scott R. Hammond,[†] Andrew J. Ferguson,[†] Benjamin J. Schwartz,[‡] and Nikos Kopidakis*[,†]

[†]National Renewable Energy Laboratory, Golden, Colorado 80401, United States

[‡]Department of Chemistry and Biochemistry and California Nanosystem Institute, University of California, Los Angeles, California 90095-1569, United States

ABSTRACT: In this work, we use the time-resolved microwave conductivity (TRMC) technique to study the dynamics of charge carrier generation in *sequentially* deposited conjugated polymer/fullerene layers. These layers are either fully solution-processed, using orthogonal solvents for the layers of the polymer poly(3-hexylthiophene) (P3HT) and the fullerene phenyl-C_{61}-butyric acid methyl ester (PCBM), or prepared by thermally evaporating a C_{60} layer onto P3HT films. Our work is motivated by the remarkable efficiency of organic photovoltaic (OPV) devices using a sequentially processed P3HT/PCBM active layer. Here we use an electrodeless photoconductivity probe, so we can photoexcite the sample either through the polymer or the fullerene layer. We use samples with extremely thick P3HT films (2.4 μm) and show that excitation from either side of both as-cast and thermally annealed sample yields virtually identical results, consistent with mixing of the PCBM into the polymer film. We also compare solution-deposited samples to samples made by thermally evaporating C_{60} on P3HT, and find that we can distinguish between charge generation in bulk-P3HT and at the polymer/fullerene interface. We show that, despite their morphological differences, the carrier dynamics in the sequentially processed samples resemble those of mixed, bulk heterojunction (BHJ) systems. All of this is consistent with the idea that PCBM readily mixes into the P3HT film in sequentially deposited P3HT/PCBM samples, although the total amount of fullerene mixed into the P3HT appears to be less than that typically used in an optimized BHJ. Finally, we discuss the implications for OPV device architectures prepared by sequential deposition from solution.

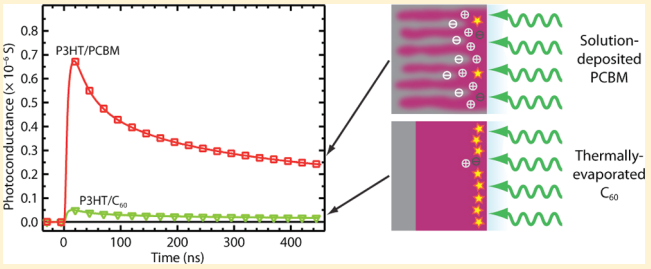

1. INTRODUCTION

Recent advances in the efficiency of solution-processed organic photovoltaic (OPV) devices[1] have transformed them from a scientific curiosity to a technologically relevant renewable source of energy using environmentally friendly materials.[2−4] The most basic method to fabricate an OPV active layer composed of a conjugated polymer and a fullerene derivative is simply to blend the two materials in a solution and cast the blend into a film. This strategy results in a composite structure that overcomes the limitation of the short exciton diffusion length (typically reported to be between 4 and 10 nm[5−8]) in the conjugated polymer by distributing the polymer−fullerene interface throughout the bulk of the film, hence the term *bulk heterojunction* (BHJ).[2,3] After light absorption, typically by the conjugated polymer component, the exciton is dissociated into free carriers at the polymer−fullerene interface; the electron is then conveyed via the fullerene network to a metal contact, and the hole is transported to the other contact via the polymer phase.[2,3]

Although a major factor in the remarkable increases in efficiency is the design of new materials tailored for enhanced harvesting of the solar spectrum, the need to optimize the method of deposition of the active layer from solution is ubiquitous. OPV devices have power conversion efficiencies (PCEs) that are critically dependent on the precise method used to deposit a film from a blend solution; varying simple processing parameters such as the solvent[9,10] or the temperature of the solution and/or substrate[11,12] or using processing additives that influence the morphology of the resulting film[13,14] can all influence the performance of BHJ devices. Recently, a new method to solution-process polymer−fullerene OPV active layers has been proposed by Ayzner et al.,[15] in which the polymer poly(3-hexylthiophene) (P3HT) and the soluble fullerene derivative phenyl-C_{61}-butyric acid methyl ester (PCBM) are deposited *sequentially* and *separately* from orthogonal solvents instead of from a mixed solution. As shown by Ayzner et al.,[15] this approach results in solar cells with a PCE of 3.5%, which is only ca. 0.2% lower than a fully

Received: December 22, 2011
Revised: February 27, 2012
Published: March 6, 2012

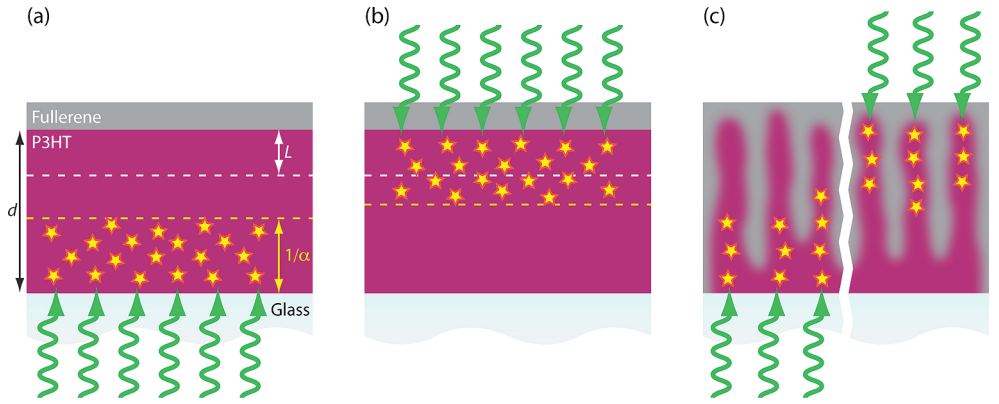

Figure 1. Photoexcitation geometries for the *sequentially* deposited organic layers: (a) excitation through the P3HT underlayer and (b) excitation through the fullerene overlayer. L is the exciton diffusion length, d is the P3HT thickness, $1/\alpha$ is the absorption depth, and the stars represent photogenerated excitons. For planar interfaces, such as the ones shown in (a) and (b), the two types of excitation can be distinguished provided that $1/\alpha \ll d - L$. (c) A sample in which the fullerene is mixed with the P3HT, to form a BHJ-like structure where the same photoresponse is expected irrespective of the direction of illumination. In the text, we refer to illumination geometry (a) and (b) to represent illumination through the substrate or through the free surface of the sample, respectively, even though the samples may not be the idealized bilayers depicted above.

optimized (and certified) BHJ OPV device with the same active materials deposited from a mixed solution.[16] Such performance is remarkable and rather surprising given that the thickness of the polymer layer ($d \approx 115$ nm) is much larger than the exciton diffusion length,[5−8] and has sparked interest in investigating the morphology and charge generation mechanisms in sequentially deposited organic layers.

Lee et al.[17] have undertaken a detailed study of the morphology of solution processed P3HT/PCBM samples formed by sequential layer deposition using a very similar approach to ref 15. By using X-ray photoelectron spectroscopy (XPS), in combination with neutron reflectometry, they found that, even with the use of orthogonal solvents and no thermal annealing, the PCBM mixes into the P3HT underlayer.[17] Surprisingly, they found that PCBM has a constant concentration profile with depth in the P3HT layer, reaching all the way to the substrate, suggesting a nondiffusive mechanism for incorporation. These authors suggested that intermixing is most likely driven by swelling of the P3HT in the solvent used to deposit the PCBM without destroying the ordered domains of P3HT, and that subsequent thermal annealing can drive the process to completion.

In addition, Treat et al.[18] used a float-casting method to prepare a free-standing P3HT film that was placed on top of a PCBM film to form a true bilayer structure. Using dynamic secondary ion mass spectrometry, they showed a clear driving force toward a homogeneous mixture of P3HT and PCBM from a distinctly heterogeneous structure even after moderate thermal annealing at 50 °C. These results strongly suggest that mixing of PCBM within P3HT occurs only within disordered regions of P3HT and has little effect on the presence or growth of the P3HT crystallites during thermal annealing, providing evidence that the fullerene phase is most likely either aggregated and/or molecularly dispersed within disordered regions of P3HT.[19]

Several other groups have attempted to construct OPV devices either by deposition of a fullerene layer onto a polymer layer through thermal evaporation of C_{60}[20−23] or by casting a fullerene-rich layer onto a polymer-rich layer from an orthogonal solvent.[24−27] This type of deposition was typically followed by thermal annealing above the glass transition temperature of the polymer, which promotes fullerene diffusion into the polymer phase, resulting in the formation of a mixed polymer/fullerene phase with the concentration of the majority carrier component located in the vicinity of the desired device contact. These device architectures have therefore been referred to as *concentration-graded bilayers*.

Although the structure of sequentially deposited polymer/fullerene films is a topic of intense interest, the dynamics of photoinduced charge generation and decay have not yet been addressed, and form the scope of this paper. Motivated from previous device work,[15] here we study polymer/fullerene samples that include the same active layers as were used in devices, with the addition of samples that would not work as an active layer in a device but allow us to understand the mixing of the polymer and fullerene components and its effect on photocarrier dynamics.

Specifically, we fabricated samples onto quartz substrates (a) by sequentially depositing the polymer and fullerene layers from solution using orthogonal solvents, dichlorobenzene (DCB) for P3HT and dichloromethane (DCM) for PCBM, and (b) by thermally evaporating the fullerene (C_{60}) onto a solution-deposited polymer film. We then used the flash-photolysis time-resolved microwave conductivity (FP-TRMC) technique to study the dynamics of charge generation and decay in these samples. Using this contactless photoconductivity probe allows photoexcitation of the sample either through the polymer or fullerene layer.

For our studies, we chose to use a thick ($d \approx 2.4$ μm) polymer film and to photoexcite the sample either through the quartz substrate (Figure 1a) or through the top PCBM layer (Figure 1b). Depending on the degree of mixing of PCBM into the polymer film, there will be an asymmetry between the two directions of excitation. If the polymer is photoexcited through the glass substrate (Figure 1a) and the absorption depth of the excitation, $1/\alpha$, is small compared to the difference of the film thickness d and the distance L over which excitons can move during their lifetime, then excitons cannot reach the polymer/fullerene interface to undergo dissociation. Thus, in this case, a photoresponse resembling that of a pure polymer film is expected, i.e., a low yield for free carrier generation and a correspondingly low photoconductance signal.[28−30] This result is expected no matter whether the excitons move by simple diffusion or via some other process, such as long-range energy

dx.doi.org/10.1021/jp212390p | J. Phys. Chem. C 2012, 116, 7293−7305

transfer.[31,32] On the other hand, if the samples are photoexcited through the fullerene overlayer (Figure 1b), a significant number of excitons will be produced within L of the polymer/fullerene interface, so enhanced free carrier generation and an increased photoconductance signal are expected, as is typically observed in donor−acceptor systems.[5,30,33−35]

With this reasoning, we also would expect that decreasing the thickness, d, of the sample will gradually diminish the asymmetry between the two directions of excitation. It is important to note, however, that this asymmetry will be preserved even if there is mixing of the two layers, provided that PCBM does not reach the region of the polymer film where photoexcitation occurs (Figure 1a). On the other hand, if PCBM diffuses all the way through the thick polymer film, as in Figure 1c, the two photoexcitation directions will become more symmetrical; i.e., both will generate excitons in the vicinity of a BHJ-like interface and result in enhanced free carrier generation in the sample. We will show that the latter is the case when the polymer and PCBM are solution-cast—little or no asymmetry is found in the magnitude of the photoconductance for the two directions of excitation, and the photoconductance transients resemble those of a P3HT:PCBM BHJ.[36]

Overall, on the basis of our analysis of photoconductance transients in sequentially deposited samples from solution, we conclude that, in addition to mixing of the fullerene in the polymer film, pure fullerene domains are also formed, whose conductance behaves in much the same way as in a BHJ. We also estimate the weight ratio of solvent-cast fullerene that mixes into a 75 nm P3HT film (similar to that used in devices by Ayzner et al.[15]) in the range of 5−20%. Literature estimates have given an effective PCBM loading of 35% in P3HT, although the P3HT film in that case was thinner (ca. 50 nm).[17] In addition, we also show that, when the fullerene layer is deposited by vacuum sublimation, strong asymmetry is found between the two directions of excitation, indicating limited or no diffusion of the thermally deposited fullerene into the polymer underlayer. Our results also confirm that annealing promotes mixing of the polymer and fullerene, no matter how they are deposited, as has been observed by others.[17,18] Finally, we discuss how our conclusions, based on contactless photoconductivity measurements, can be used to understand the operation of complete OPV devices with a sequentially deposited P3HT/PCBM active layer.

2. EXPERIMENTAL SECTION

2.1. Sample Preparation. In the following, we will use the notation P3HT/fullerene to denote a sample where the P3HT and fullerene have been deposited *sequentially*, whereas BHJ samples deposited from a blend solution are referred to as P3HT:fullerene. For the P3HT/fullerene films in this work, both solution-deposited PCBM and thermally evaporated C_{60} were used. The fabrication of fully solution-processed organic bilayers requires finding a set of orthogonal solvents[37] such that the solvent used to deposit the fullerene overlayer does not dissolve the polymer underlayer. For P3HT/PCBM samples, we used dichloromethane (CH_2Cl_2) for this purpose because PCBM is reasonably soluble in DCM and the solubility of P3HT in DCM is very low, making it possible to spin-coat PCBM layers on top of P3HT.[15] In some cases, as-received P3HT was pretreated (washed) in DCM by extracting a significant amount of P3HT with some DCM solvent prior to deposition of the polymer film, as described in more detail below.

Films for photoconductance measurements were deposited onto 10 mm × 24 mm quartz substrates that were cleaned by subsequent ultrasonic baths in deionized water for 5 min, and acetone and isopropanol for 20 min each. The substrates were then blown dry with N_2 gas and briefly treated with an oxygen plasma (800 mTorr for 5 min) prior to the deposition of the polymer layer. We prepared solutions of regioregular P3HT (Rieke/BASF P100 Sepiolid, $M_W \sim 50\,000$ g/mol) in dichlorobenzene (DCB) at concentrations of 25 and 50 mg/mL in order to obtain the targeted thickness. The solutions were stirred for at least 24 h at 60 °C on a digitally controlled hot-plate in a N_2-filled glovebox before being cooled to room temperature and deposited onto the quartz substrates.

Thick, drop-cast films (2.4 ± 0.4 μm) of P3HT (both as-received and washed in DCM) were used throughout this study, except for the experiments described in section 3.4 where the thickness of the P3HT film was varied to provide a comparison with device-relevant active layers. These thinner films were deposited by spin-coating at different speeds, producing P3HT films with thicknesses of 75 ± 5, 470 ± 71, and 800 ± 105 nm, as determined by a Dektak profilometer. Prior to deposition of the fullerene overlayer, freshly deposited P3HT films were allowed to dry slowly in a covered Petri dish in a N_2 atmosphere overnight for the spin-deposited films and for approximately 5 days for the drop-cast films.

Following Ayzner et al.,[15] we prepared solutions of PCBM (Nano-C) in DCM at a concentration of 10 mg/mL; since the boiling point of DCM is about 40 °C, the 10 mg/mL solution was stirred for at least 24 h at 35 °C and briefly heated up to 40 °C to ensure maximal dissolution. The PCBM solution in DCM was filtered prior to spin-coating 10 μL at 4000 rpm for 10 s onto the P3HT films, producing a PCBM overlayer with a nominal thickness of ∼34 nm, based on a previous report.[15] As a control, we also solution-deposited C_{60} following the same procedure as for the PCBM overlayer. We used a nominal concentration of 10 mg/mL of C_{60} in DCM, which corresponds to an ∼25% increase in the molar concentration of C_{60} relative to PCBM. However, much of the powder remained undissolved, due to the poor solubility of C_{60}, and for this reason, it is difficult to quantify the amount of fullerene deposited, and therefore to predict the relative fullerene loading upon mixing into the P3HT underlayer. Despite this, the solubility was still sufficient to provide a qualitative comparison of TRMC data for sequentially deposited samples using both C_{60} and PCBM.

In addition to the solution-deposited C_{60} and PCBM overlayers, we also created fullerene overlayers by thermal evaporation of C_{60} powder onto P3HT films. In this case, the P3HT films were kept in a vacuum (∼10^{-5} mbar) for at least 2 h prior to the evaporation of C_{60} at a rate of 2 Å/s, producing C_{60} overlayers of 20 ± 2 nm. Neat films of P3HT, PCBM, and C_{60} were also deposited for comparison.

Finally, we prepared P3HT:PCBM BHJ blends with 1, 5, 20, and 50% by weight PCBM loading in order to compare with bilayer samples and make an assessment of the effective fullerene loading in the *sequentially* solution-deposited samples. BHJ solutions were prepared with a total active material content of 7.5 mg/mL in chloroform and were stirred overnight at 50 °C under a nitrogen atmosphere. The blends with different PCBM loadings were then drop-cast onto clean, O_2-plasma-treated quartz substrates and allowed to dry slowly, followed by subsequent annealing at 50 °C for 1 min to remove any residual solvent from the blend.

2.2. P3HT Treatment. To ensure that the solvents used in our sequential deposition technique were as orthogonal as possible, for some of our samples, we extracted P3HT with DCM prior to film deposition in order to remove any portion of the material that was soluble in DCM. To do this, we placed 300 mg of the as-received P3HT (Rieke/BASF P100 Sepiolid, $M_W \sim 50\,000$ g/mol) powder in a 500 mL beaker with DCM solvent and stirred at room temperature for several days. The solid material that remained undissolved was then collected from the solution by filtration and dried overnight under a vacuum at room temperature. We refer to this material as *washed* P3HT and denote it as *w*-P3HT hereafter. The remaining DCM solution, which included the portion of the P3HT powder that dissolved in DCM, was also collected for subsequent molecular weight analysis.

Gel permeation chromatography (GPC) analysis was performed on both the as-received and washed P3HT as well as on the DCM-extracted P3HT, in order to examine the effect of the P3HT washing procedure on the molecular weight distribution of the polymer. To do this, solutions of the three P3HT polymer samples (as-received, washed, and the solution extract) were prepared at 1 mg/mL in chloroform and allowed to stir at 50 °C on a digitally controlled hot-plate in a N_2-filled glovebox for ~24 h before cooling to room temperature and filtering through a 1.0 μm PTFE syringe filter. The 50 μL samples were then injected into an Agilent LC1200 liquid chromatography system and passed through a PLgel 5 μm MIXED-D column (300 mm × 7.5 mm i.d.) with HPLC-grade chloroform eluent at 1 mL/min. Detection was accomplished with an Agilent 1200 series refractive index detector (RID) at 35 °C, with calibration of retention time against Agilent polystyrene standards.

2.3. Photoconductance Measurements. The photoconductance of the samples was measured using the flash-photolysis time-resolved microwave conductivity (FP-TRMC) technique, which has been described previously.[5,28−30,33,34] An advantage of this technique is that it does not require electrical contacts, which is critical to this study because measurements of polymer/fullerene films can be performed following photoexcitation of the sample through either the polymer or fullerene layer in order to investigate the importance of excitation of the polymer both a long distance from and at the polymer/fullerene interface (see Figure 1). The concept of illuminating bilayer samples from either side and using TRMC to probe photoinduced carrier generation has previously been used to determine the exciton diffusion length in P3HT,[5] where a compact TiO_2 underlayer was used as the electron acceptor, providing a planar exciton-dissociating interface.

The samples are placed in a resonance cavity at the end of an X-band microwave waveguide, and the time-dependent change of the microwave power in the cavity, $\Delta P(t)$, due to transient changes in the conductance of the samples upon illumination with 5 ns laser pulses was monitored with nanosecond resolution. The laser pulse source was an Optical Parametric Oscillator (OPO − Continuum Panther) pumped by the 355 nm harmonic output of an Nd:YAG laser (Continuum Powerlite). The OPO was tuned to 500 nm for excitation of the polymer, and samples were measured with the pump beam incident either on the air/quartz or air/fullerene interface, i.e., through the polymer or through the fullerene layer, respectively. The samples were measured both as-deposited and after thermal annealing at 150 °C for 20 min on a digitally controlled hot-plate in a N_2 atmosphere. The beam was diverged to the measuring cell to ensure a uniform profile over the whole sample, and the typical laser fluence was ca. 3.5 mJ/cm^2/pulse; for transients measured at lower excitation intensities, the pulse power was attenuated with a series of neutral density filters.

The time-dependent change in the microwave power absorbed by the sample is related to the photoinduced conductance, $\Delta G(t)$, of the films by[5,28−30,33,34]

$$\Delta G(t) = -\frac{1}{K}\frac{\Delta P(t)}{P} \tag{1}$$

where K is an experimentally determined calibration factor derived from the resonance characteristics of the cavity and the dielectric properties of the sample. The response of the resonant microwave cavity is 6−10 ns and depends on the type of sample measured; this is taken into account in our analysis and discussed in more detail in section 3.4.

The end-of-pulse (EOP, or peak) value of the measured photoconductance is related to the product of the quantum yield (ϕ) for mobile charge carrier generation per absorbed photon under the 5 ns long pulses and the sum of the electron and hole mobilities ($\sum\mu = \mu_e + \mu_h$) by

$$\Delta G_{EOP} = \beta q_e I_0 F_A[\phi \sum \mu] \tag{2}$$

where I_0 is the incident photon flux, F_A is the fraction of incident light absorbed by the film, β is the ratio between the broad and narrow inner dimensions of the waveguide used, and q_e is the elementary charge. At low absorbed photon flux, ΔG_{EOP} increases linearly with I_0; however, as the light intensity increases, higher-order processes occur that limit the carrier generation yield, ϕ, and the dependence becomes sub-linear.[28,30] We use the empirical relationship given in eq 3 to extrapolate to the linear response limit of the photoconductance at low excitation intensities:

$$\Delta G_{EOP} = \frac{AI_0F_A}{1 + \sqrt{BI_0F_A} + CI_0F_A} \tag{3}$$

where A, B, and C are fitting parameters.[38] Comparison of eqs 2 and 3 allows us to obtain the linear response limit as $A = \beta q_e[\phi\sum\mu]$.

3. RESULTS AND DISCUSSION

3.1. P3HT Pretreatment. To begin, we discuss the effects of the P3HT washing procedure on the molecular weight distribution of the polymer, which we investigated using gel permeation chromatography (GPC) as shown in Figure 2. Washing with DCM predominately removes lower molecular weight material, as seen from the trace for the DCM-extracted portion of the material (gray triangles), causing the molecular weight distribution of the washed, *w*-P3HT (green squares), sample to shift to higher molecular weights compared to the as-received sample (red circles).

In addition to GPC, we have also performed several control experiments (data not shown) in order to check whether the application of DCM solvent during spin-coating of the PCBM overlayer would change the properties of the P3HT film underlayers. The first experiment consisted of measuring the absorption spectra of as-received P3HT and the *w*-P3HT films, both prior to and after spin-coating a drop of 10 μL of DCM solvent on the film surface at 4000 rpm for 10 s. Compared to the films without the DCM drop, the films with a drop of DCM solvent showed a slightly lower OD, ca. 5 and 7% lower,

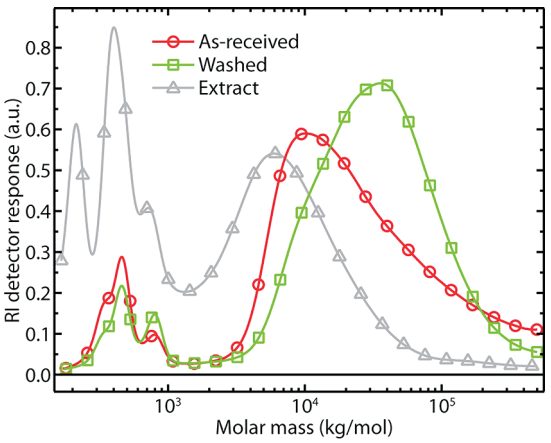

Figure 2. Gel permeation chromatograms for as-received, washed- (DCM-insoluble), and extract- (DCM-soluble) P3HT.

respectively, for the *w*-P3HT and P3HT that we attribute to a removal of some of the P3HT material on the surface that is soluble in DCM. This result also suggests that there is still a small amount of soluble fractions of *w*-P3HT that is potentially soluble in DCM. We note that a smaller drop (1−2%) in OD was observed by Ayzner et al.[15] when DCM was spun onto the P3HT film. In that report, the authors utilized a double extraction method that effectively removed a larger fraction of the polymer that was soluble in DCM.

The second control experiment consisted of measuring the photoconductance by TRMC of the *w*-P3HT and the as-received P3HT where we observed nearly identical results for both films, indicating similar photocarrier generation and decay dynamics in the two samples.

3.2. TRMC of P3HT/Fullerene Samples with *Thick* P3HT. In this section, we present TRMC results of P3HT/PCBM and P3HT/C_{60} samples with P3HT film underlayers that are all ca. 2.4 μm thick. In Figure 3, we show photoconductance transients measured by TRMC for unannealed P3HT/PCBM and P3HT/C_{60} films compared to a 1:1 by weight P3HT:PCBM blend (black traces); the response for a neat P3HT film (gray traces) is also shown for comparison. We note that for this sample thickness all excitation photons are absorbed; therefore, comparison between the samples can be carried out without normalizing the photoconductance transients by the fraction of light absorbed. Figure 3a shows ΔG transients for samples excited from the substrate side (the illumination geometry of Figure 1a). The high photoconductance observed in the P3HT:PCBM BHJ sample compared to the pure P3HT film is attributed to two factors: (1) the increase of the yield for free carrier generation, ϕ (eq 2), when the acceptor is present, and (2) the contribution to $\sum\mu$ (eq 2) of the mobility of electrons in PCBM domains, as

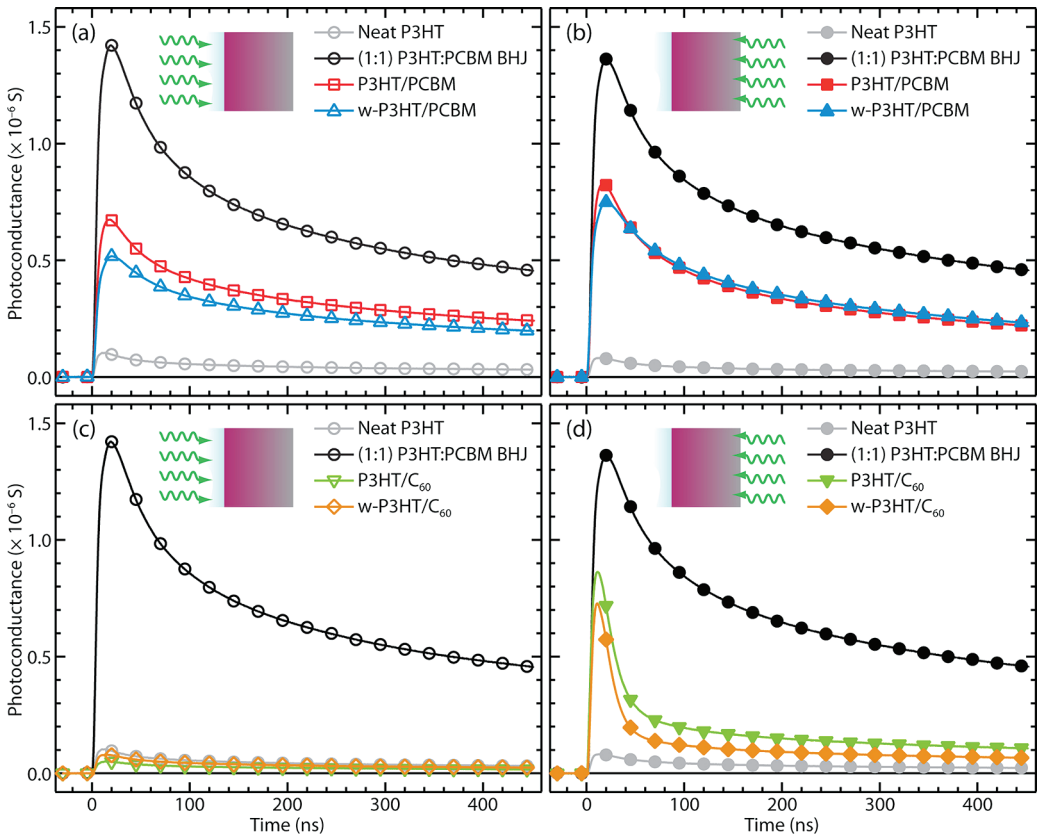

Figure 3. Photoconductance decay transients for sequentially deposited P3HT/fullerene samples illuminated through the substrate (left) and through the fullerene overlayer (right): cartoons show the illumination geometry. (a and b) Solution-deposited PCBM overlayer, on either as-received (red squares) or washed (blue triangles) P3HT. (c and d) Thermally evaporated C_{60} on as-received (green triangles) or washed (orange diamonds) P3HT. Also shown for comparison are transients for neat P3HT (gray circles) and a 1:1 P3HT:PCBM bulk heterojunction (black circles). In all cases, the P3HT underlayer thickness was ~2.4 μm, the samples were not thermally annealed, the excitation wavelength was 500 nm, and the absorbed photon flux was ca. 5×10^{15} cm^{-2}.

dx.doi.org/10.1021/jp212390p | J. Phys. Chem. C 2012, 116, 7293−7305

has been documented in detail previously.[35,36] Pure P3HT is an excitonic semiconductor with a low ϕ of ca. 2%[28−30] and a $\sum\mu$ that is dominated by the mobility of holes in the polymer, measured to be 0.014 $cm^2/(V{\cdot}s)$ using pulse-radiolysis TRMC.[39] When PCBM is added in a BHJ structure, ϕ increases to ca. 90%[36] and $\sum\mu$ now also includes the mobility of electrons in PCBM, which has been estimated to be in the range 0.014−0.064 $cm^2/(V{\cdot}s)$ depending on the PCBM loading.[36]

When examining the transients in Figure 3, it is important to remember that laser pulses of 500 nm entering the P3HT/PCBM sample through the substrate are absorbed within ∼100 nm of the quartz/P3HT interface. Thus, it is somewhat surprising that the magnitude of the photoconductance of the sequentially deposited sample using as-received P3HT (red trace) is about a factor of 8 larger than that of the pure polymer. A small drop in ΔG is observed when *w*-P3HT is used (blue trace); however, ΔG for the *w*-P3HT/PCBM films is still about a factor of 7 larger than that of pure P3HT. This increase in ΔG for the sequentially solution-deposited films is thus indicative of mixing of the PCBM into the 2.4 μm thick P3HT underlayer to a depth within 100 nm of the substrate.

To understand the degree to which PCBM mixes with the P3HT underlayer, Figure 3b explores the nature of the photoconductance transients obtained following excitation of these same samples through the top PCBM layer (geometry of Figure 1b). Comparison of the black curves in Figure 3a and b shows that the photoconductance transients for the BHJ sample are identical for both excitation geometries, as expected for a homogeneous, symmetric sample. In contrast, there is an increase of the photoconductance of the P3HT/PCBM and *w*-P3HT/PCBM samples when they are photoexcited through the top (fullerene) layer relative to when they are excited through the substrate. This indicates that there is less fullerene in the vicinity of the substrate in the sequentially solution-processed samples than there is at the top interface where the PCBM was deposited.

Figure 3c compares photoconductance transients for the excitation geometry in Figure 1a of samples of pure P3HT (gray trace), P3HT:PCBM BHJ (black trace), and P3HT/C_{60} (green and orange traces), where the C_{60} was deposited by thermal evaporation. The magnitude of the ΔG transient for the P3HT/C_{60} films, with both as-received P3HT and *w*-P3HT, is almost identical to that for pure P3HT. This is consistent with the idea that any mixing of thermally evaporated C_{60} into the thick P3HT underlayer film is either nonexistent or limited to a region close to the interface. In contrast, Figure 3d shows that photoexciting these samples through the top C_{60} layer (geometry of Figure 1b) results in a significantly higher peak photoconductance signal, as would be expected for an enhanced free carrier yield because excitons are generated close to the P3HT/C_{60} interface.

To further analyze the nature of PCBM mixing in our samples, we use the peak of the photoconductance transient, ΔG_{EOP}, as a probe of the yield of photocarrier generation during the laser pulse. These values are plotted in Figure 4 against the absorbed photon flux (I_0F_A) for samples illuminated through the quartz substrate. All samples exhibit the well-documented sublinear dependence of ΔG_{EOP} on I_0F_A, which is caused by the quenching of excitons by free charge carriers at high excitation intensities.[30,36] The peak photoconductance of the P3HT/PCBM and *w*-P3HT/PCBM is about an order of magnitude higher than that of P3HT throughout the range of

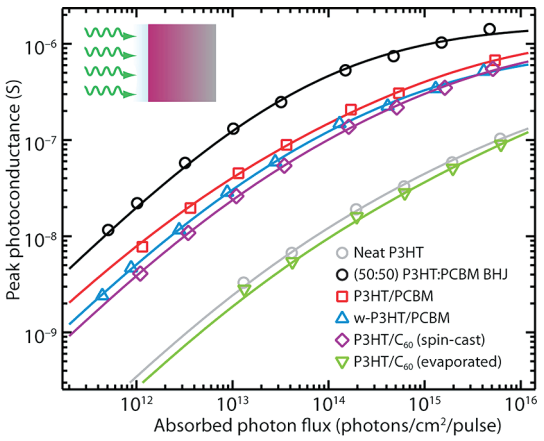

Figure 4. The peak (or end of pulse) photoconductance values as a function of absorbed photon flux for sequentially deposited P3HT/fullerene samples: solution-deposited PCBM overlayer, on either as-received (red squares) or washed (blue triangles) P3HT, solution-deposited C_{60} overlayer on as-received P3HT (purple diamonds), and thermally evaporated C_{60} overlayer on as-received P3HT (green triangles). Also shown for comparison are the peak photoconductance values for neat P3HT (gray circles) and a 1:1 P3HT:PCBM bulk heterojunction (black circles). The standard deviations of the abscissa and ordinate values correspond to ∼15% of the value, determined from the standard deviation of the laser pulse energy (error bars are omitted for clarity, since they are comparable to the size of the symbols), and the solid lines are fits to the data using eq 3. Illumination was performed through the substrate, as depicted in the cartoon, at a wavelength of 500 nm.

intensities. Figure 4 also shows that ΔG_{EOP} of the P3HT/C_{60} sample with evaporated C_{60} is within the experimental error of the photoconductance of the pure P3HT sample. The differences in the magnitude of ΔG_{EOP} observed between the solution-cast PCBM layer in the P3HT/PCBM sample and the thermally evaporated C_{60} layer in the P3HT/C_{60} sample indicate a difference in the morphology of this sample: vacuum deposition of C_{60} limits or entirely prevents mixing with the P3HT film, at least for samples that have not been annealed (*vide infra*).

In order to verify that solution-casting of the fullerene is the cause of the difference between the morphology and thereby the photoconductance of the P3HT/PCBM and P3HT/C_{60} samples, we carried out an additional experiment in which we cast C_{60} onto P3HT from a 10 mg/mL DCM solution using identical deposition conditions to that for PCBM (see the Experimental Section for details). The magnitude of ΔG_{EOP} for that sample (also shown in Figure 4) is comparable to the solution-cast P3HT/PCBM films. Clearly, whenever the fullerene (PCBM or C_{60}) is *cast from solution*, the increase of ΔG_{EOP} relative to the pure polymer is caused by mixing of the fullerene into the P3HT film, consistent with independent structural studies of sequentially deposited polymer/fullerene layers.[17,18] We note that the rather extreme thickness (ca. 2.4 μm) of the polymer layer in the samples used to collect the data shown in Figure 4 is at least 2 orders of magnitude larger than the length of exciton diffusion in P3HT (4−10 nm)[5−8] and previously reported characteristic length scales for exciton transfer by Förster processes (ca. 11 nm).[32] Therefore, mixing of the fullerene into the polymer is the only plausible explanation for the increased photoconductance of solution-cast P3HT/fullerene samples when they are photoexcited under the scheme shown in Figure 1a. The data of Figure 4 also

dx.doi.org/10.1021/jp212390p | J. Phys. Chem. C 2012, 116, 7293−7305

show that prewashing the P3HT with DCM has relatively little effect on the mixing of solution-cast fullerene into it, lending further support to the hypothesis that swelling of the amorphous P3HT regions by the DCM is what drives fullerene mixing in solution-processed multilayer films.[17,40] Finally, we also verified that spin-coating pure DCM onto a P3HT film did not result in any significant change in the photoconductance (data not shown).

In summary, we conclude that the scheme depicted in Figure 1a is only applicable when the fullerene is thermally evaporated onto P3HT. For fullerenes, either PCBM or C_{60}, deposited *from DCM solution* onto P3HT, the resulting geometry is something approaching that illustrated in Figure 1c.

3.3. Effects of Thermal Annealing on the Mixing of Solution-Processed P3HT/PCBM Films. Although we only have discussed as-cast films, previously it was shown that thermal annealing of P3HT/PCBM films leads to a significant photovoltaic performance improvement.[15] Structural work also has suggested that thermal annealing drives additional PCBM from the solution-cast overlayer into the P3HT underlayer, even though the extent of photoluminescence quenching for the P3HT/PCBM samples is *smaller* following thermal annealing.[17] Thus, in this section, we discuss the effects of thermal annealing on the photoconductance response; the samples were annealed in an inert atmosphere at 150 °C for 20 min.

In order to obtain the low-intensity limit for the $\phi\sum\mu$ product, we fit the ΔG_{EOP} vs I_0F_A data of Figure 4 with eq 3 at low light intensities where higher-order processes are negligible.[28,30] The results for the P3HT/fullerene samples with thick (2.4 μm) P3HT underlayers that were excited through the quartz substrate are shown in Figure 5. The value of $\phi\sum\mu$ obtained here for P3HT and for the P3HT:PCBM BHJ is in good agreement with previous work.[28−30,35,36] We note that the low intensity limit of $\phi\sum\mu$ for the sequentially deposited P3HT/PCBM sample is ca. 0.04 $cm^2/(V{\cdot}s)$, which means that (since the free carrier yield cannot exceed unity, $\phi <$ 1) the lower limit of the sum of the mobilities is 0.04 $cm^2/(V{\cdot}s)$. As we will discuss in more detail below, the hole mobility in P3HT has been found to be 0.014 $cm^2/(V{\cdot}s)$;[39] therefore, $\phi\sum\mu$ includes a substantial contribution from electron mobility, indicating that PCBM aggregates are formed during mixing with the P3HT film. These values correspond to the *high-frequency mobility* measured with the 9 GHz microwave probe beam and should not be directly compared to mobilities measured using device methods such as photocarrier time-of-flight (TOF) or charge extraction by a linearly increasing voltage (CELIV).

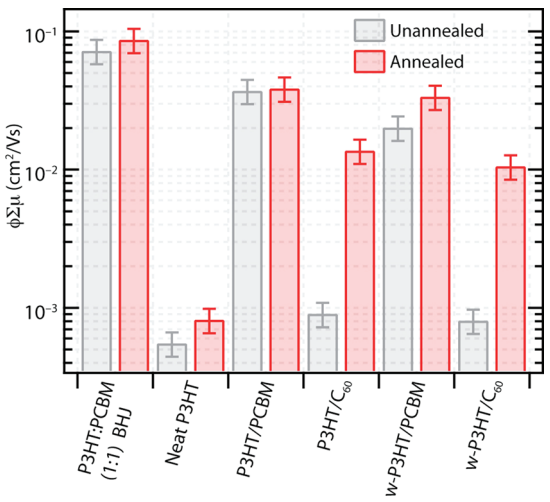

Figure 5. The product of the quantum yield (ϕ) for mobile charge carrier generation and the sum of the mobilities ($\sum\mu$) for neat P3HT, a (1:1) P3HT:PCBM bulk heterojunction, and sequentially deposited polymer/fullerene layers with a combination of either solution-deposited PCBM or evaporated C_{60} overlayers and P3HT or *w*-P3HT underlayers. Illumination was performed through the substrate at a wavelength of 500 nm.

The data in Figure 5 also show that only small changes are observed in the photoconductance of P3HT and the P3HT:PCBM BHJ after annealing. Despite the dramatic processing-induced changes observed in the performance of photovoltaic devices with P3HT:PCBM BHJ active layers,[41] TRMC is a local photoconductivity probe that does not require long-range percolation of charge carriers and is therefore relatively insensitive to annealing. Furthermore, our BHJ sample was drop-cast and the slow drying process has essentially replicated the effect of thermal annealing.

In the case of the *w*-P3HT/PCBM sample, however, $\phi\sum\mu$ increases with annealing, indicating that prewashing the P3HT with DCM decreases the total amount of PCBM that mixes into the underlayer during solution deposition of the PCBM overlayer, consistent with the idea that the fullerene only penetrates into amorphous regions of the P3HT. After the annealing step, diffusion of PCBM is promoted, and $\phi\sum\mu$ for the *w*-P3HT/PCBM sample reaches the same value (within error) as the P3HT/PCBM sample with untreated P3HT.

3.4. Analysis of Photoconductance Decay Transients. The photoconductance transients of Figure 3 show that mobile photoinduced carriers are detected at time scales greater than 100 ns, well beyond the ~5 ns width of the laser excitation pulse. The collection time of photoinduced carriers in an OPV device under operating conditions ranges from hundreds of ns to μs;[30] therefore, our results show that in the sequentially processed samples the carriers survive long enough to be collected as photocurrent under a built-in field in an OPV device, provided there is a percolation pathway for the electrons (*vide infra*). Interestingly, the fact that the photoinduced carriers are so long-lived, even in the absence of the built-in fields present in an operating device, suggests that the microstructure formed in sequentially deposited samples hinders carrier recombination at the P3HT−fullerene interface. A recent experimental study of P3HT:PCBM blends suggested that a reduced recombination rate resulted from an energetic barrier at the interface,[36] which was also recently predicted theoretically, using a combination of classical molecular dynamics and quantum chemical calculations to study the electronic structure of P3HT at the interface with PCBM.[42]

In the following, we use the end-of-pulse (peak) values of the photoconductance obtained in the previous section as input for a quantitative analysis of the time dependence of ΔG; in what follows, we focus on the conductance dynamics during the first 450 ns in our P3HT/fullerene samples. The values of $\phi\sum\mu$ presented in the previous section can be used to make an estimation of the quantum yield for carrier production (ϕ) if the sum of the mobilities ($\sum\mu = \mu_e + \mu_h$) is known. In previous pulse radiolysis TRMC studies of pristine P3HT, carrier transport was dominated by mobile holes and $\mu_{h,P3HT}$ was found to be 0.014 $cm^2/(V{\cdot}s)$.[39] This value has also provided a

dx.doi.org/10.1021/jp212390p | J. Phys. Chem. C 2012, 116, 7293−7305

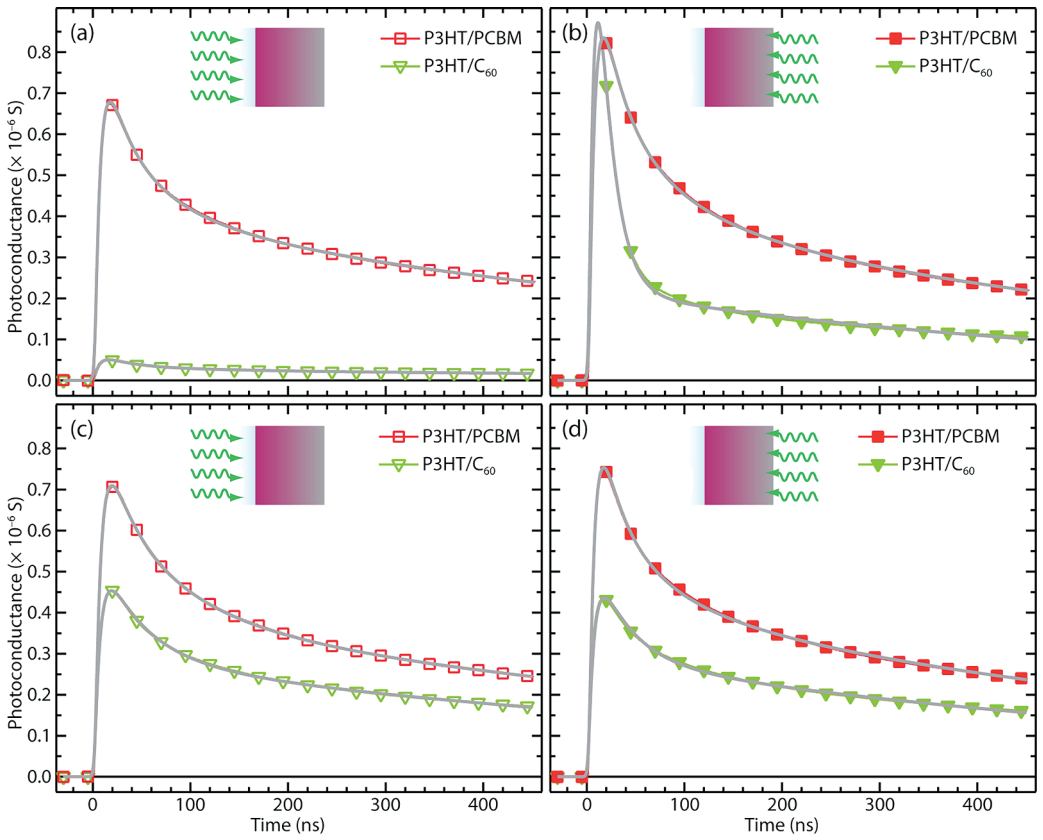

Figure 6. Photoconductance decay transients for sequentially deposited P3HT/fullerene samples, solution-deposited PCBM (red squares), and thermally evaporated C_{60} (green triangles), illuminated through the substrate (left) and through the fullerene overlayer (right): cartoons show the illumination geometry. The top panels show transients for the unannealed samples and the bottom panels for samples annealed at 150 °C for 20 min. The solid gray lines indicate fits to the data using eqs 4, 5, and 8.

consistent interpretation of TRMC results under pulsed laser excitation.[30,36]

We have previously developed a methodology for the analysis of TRMC transients in P3HT:PCBM blends,[30] and have applied this analysis to BHJs with varying loading ratios of PCBM.[36] The latter resulted in values for $\sum\mu$ in BHJ in the range 0.03−0.08 $cm^2/(V{\cdot}s)$, and are in agreement with values reported by others.[35] In order to carry out analysis of the photoconductance transients in this work, we chose to use an average value of $\sum\mu_{blend}$ = 0.05 $cm^2/(V{\cdot}s)$ as the sum of the mobilities in blend, or blend-like, samples. We emphasize that the conclusions presented below are virtually insensitive to variations of the chosen value for the sum of the mobilities within the reasonable range given above that spans the values reported using TRMC in P3HT:PCBM BHJs.[33,35,36]

Our analysis of the photoconductance transients is based on the observation that the experimentally measured $\Delta G_{exp}(t)$ is the convolution of the actual photoconductance, $\Delta G(t)$, with the response function of the microwave cavity, $F(t)$:[30]

$$\Delta G_{exp}(t) = F(t) \otimes \Delta G(t) \tag{4}$$

where $\Delta G(t) \propto q_e[n_h\mu_h + n_e\mu_e]$ and $F(t)$ is given by[30]

$$F(t) = N\left[\exp\left(-\frac{t-\bar{t}}{\tau_{rise}}\right) + \exp\left(\frac{t-\bar{t}}{\tau_{decay}}\right)\right]^{-1} \tag{5}$$

where τ_{rise} is the rise and τ_{decay} the decay time of the cavity response centered around $\bar{t}$ and N is a normalization factor.

Although $\Delta G(t)$ formally includes contributions to the photoconductance from both electrons and holes in the material system under investigation, for the samples studied here, one of the two charge carriers will dominate the signal if its mobility is higher. Specifically, in pure P3HT, the primary contributors to $\Delta G(t)$ are the holes with a mobility of ca. 0.014 $cm^2/(V{\cdot}s)$,[39] while a P3HT:PCBM BHJ has a higher electron mobility in the PCBM domains (0.04−0.08 $cm^2/(V{\cdot}s)$),[35,36] making electrons the dominant carrier in the photoconductance signal.

This observation allows us to formulate a simple model for $\Delta G(t)$ as follows. If we assume that the decay of the dominant carrier after photoexcitation is due to competing first- and second-order loss processes, we arrive at

$$\frac{d[n]}{dt} = -k[n] - \gamma[n]^2 \tag{6}$$

where k and γ are, respectively, rate coefficients that describe the first- and second-order loss processes and n is the dominant charge carrier density. Using the solution of eq 6 for the carrier density, we obtain the following expression for the photoconductance:

$$\Delta G(t) = \beta q_e d\left(\sum\mu\right)\left[\frac{kn_0}{(k+\gamma n_0)e^{kt} - \gamma n_0}\right] \tag{7}$$

where n_0 is the charge density at t = 0, d is the penetration depth of the photoexcitation, and the other parameters were defined in the Experimental Section. A complete analysis of the

dx.doi.org/10.1021/jp212390p | J. Phys. Chem. C 2012, 116, 7293−7305

Table 1. Parameters Obtained from Global Analysis of Excitation Intensity-Dependent Photoconductance Transients for Various P3HT−Fullerene Samples

experimental conditions and sample[a]			k^b ($\times 10^7$ s^{-1})	γ^c ($\times 10^{-12}$ cm^3/s)	ϕ^d (%)
control		P3HT	4.0 ± 2.7	71 ± 21	9 ± 4
		BHJ	2.6 ± 1.4	11 ± 6	90 ± 12
excitation through quartz−film interface	unannealed	*w*-P3HT/PCBM	2.6 ± 1.0	21 ± 8	40 ± 12
		w-P3HT/C_{60}	4.0 ± 0.8	85 ± 24	6 ± 3
		P3HT/PCBM	3.1 ± 1.1	25 ± 9	74 ± 22
		P3HT/C_{60}	4.0 ± 2.6	79 ± 22	7 ± 3
	annealed	*w*-P3HT/PCBM	2.7 ± 1.0	17 ± 6	68 ± 20
		w-P3HT/C_{60}	3.3 ± 1.1	25 ± 9	24 ± 6
		P3HT/PCBM	2.6 ± 0.9	14 ± 5	77 ± 23
		P3HT/C_{60}	4.8 ± 1.8	10 ± 4	27 ± 8
excitation through air−film interface	unannealed	*w*-P3HT/PCBM	2.2 ± 0.8	12 ± 4	86 ± 25
		w-P3HT/C_{60}	21 ± 7	3.5 ± 1.2	25 ± 7
		P3HT/PCBM	2.8 ± 1.0	19 ± 7	81 ± 24
		P3HT/C_{60}	16 ± 5	9 ± 3	35 ± 10
	annealed	*w*-P3HT/PCBM	2.8 ± 0.9	18 ± 6	75 ± 20
		w-P3HT/C_{60}	3.4 ± 1.3	18 ± 7	23 ± 7
		P3HT/PCBM	3.1 ± 1.1	25 ± 9	66 ± 20
		P3HT/C_{60}	6.3 ± 2.2	10 ± 4	17 ± 5

[a] C_{60} is evaporated for all P3HT/C_{60} samples, and PCBM is solution-deposited for all P3HT/PCBM samples. [b] Rate coefficient describing the first-order decay of carriers. [c] Rate coefficient describing the second-order decay of carriers. [d] Carrier quantum yield estimated using a sum of mobilities of 0.05 $cm^2/(V{\cdot}s)$ in the blend and 0.014 $cm^2/(V{\cdot}s)$ in pure P3HT.

photoconductance of P3HT:PCBM BHJs, that includes the influence of the dark (equilibrium) carrier density in P3HT, has been presented elsewhere and is beyond the scope of this work.[36] We have found that the simplified kinetic scheme represented by eq 6 can adequately describe the early time (<100 ns) carrier dynamics, which are associated with the re-establishment of equilibrium between trapped and mobile carriers that is perturbed by the laser pulse.[36] However, an additional empirical exponential term is required to account for the full decay at longer times (up to 480 ns), and describes the trap-limited recombination of carriers. On the basis of eq 7, we have therefore formulated the following semiempirical equation for $\Delta G(t)$:

$$\Delta G(t) = \beta q_e d\left(\sum \mu\right)\left[\frac{kn_0}{(k+\gamma n_0)e^{kt} - \gamma n_0} + n_{emp}e^{-k_{emp}t}\right] \quad (8)$$

where the ad-hoc empirical exponential term is described by the parameters n_{emp} and k_{emp}.[30]

In previous work, we have used this methodology as a purely empirical means to extract the actual $\Delta G(t)$ from measured $\Delta G_{exp}(t)$ transients.[30] Here we use it to compare the time profile of the decays of $\Delta G(t)$ of P3HT/PCBM, P3HT/C_{60}, and BHJ samples and determine the factors governing the photoconductance decay dynamics in each case.

We use eqs 4, 5, and 8 to perform a global fit of the light-intensity-dependent transients for each sample, i.e., the rate coefficients k, γ, and k_{emp} are *"shared"* for all excitation intensities, and only n_0 and n_{emp} are allowed to vary independently, since only the initial charge carrier densities should vary with excitation intensity. Using a series of transients with excitation density varying by ca. 4 orders of magnitude in this global fitting scheme allows us to extract meaningful rate coefficients for the photoconductance decay in each sample.

In Figure 6, we show data for two representative samples, *w*-P3HT/C_{60} and *w*-P3HT/PCBM, and the corresponding fits, the quality of which are representative of those obtained for all samples at all measured light intensities.

Table 1 summarizes the results of the fitting process for all the samples, which allows us to quantitatively compare the profiles of the photoconductance decays for different samples. The parameters k and γ in Table 1 are first- and second-order rate coefficients that we attribute to establishment of an equilibrium between trapped and mobile carriers[36] and a recombination process, respectively. We observe that the rate coefficient related to the second-order decay, γ, in P3HT:PCBM BHJ is lower by a factor of 7 compared to that in pure P3HT. We attribute this to a slower recombination mechanism in the blend, as a result of the spatial separation of the electron and the hole into two different phases. A detailed discussion of the underlying photophysics is beyond the scope of this paper and will be reported in a forthcoming publication. We note, however, that the decrease of γ is a "fingerprint" of the presence of phase-separated fullerene and P3HT domains within or close to the region described by the excitation profile.[36] In the following, we will use the magnitude of the second-order rate coefficient γ to discuss the photoconductance decay of the P3HT/fullerene samples compared to pure P3HT and to the BHJ film.

Table 1 shows that, for the unannealed polymer/C_{60} samples excited through the quartz substrate (Figure 1a), γ is comparable to that obtained for pristine P3HT (~80 × 10^{-12} cm^3/s cf. 71 × 10^{-12} cm^3/s). This suggests the free carriers are

dx.doi.org/10.1021/jp212390p | J. Phys. Chem. C 2012, 116, 7293−7305

generated in the P3HT under the scheme of Figure 1a, as discussed above, following a P3HT-like evolution over the 450 ns of the TRMC experiment. Thermal annealing significantly reduces γ (<25 × 10^{-12} cm^3/s), so that it is now of the same order of magnitude as that obtained for a 50:50 P3HT:PCBM BHJ. This is consistent with the conclusion of section 3.3, where it was shown that thermal annealing at 150 °C for 20 min is sufficient to promote effective fullerene interdiffusion, resulting in the formation of a BHJ-like morphology. It is also interesting to note that γ for the P3HT/C_{60} sample decreases after thermal annealing more dramatically than for the w-P3HT/C_{60} sample. This implies that the fullerene molecules diffuse more easily through the polymer domain when shorter-chain polymer molecules are still present. For all solution-cast PCBM overlayers, both unannealed and annealed, γ is at least a factor of 3 smaller than for the pristine polymer; additionally, washing the polymer prior to sample preparation has no discernible impact on the magnitude of γ.

For all samples, reversal of the photoexcitation geometry, Figure 1b or top excitation in Figure 1c, results in the generation of large exciton densities close to the P3HT–fullerene interface, which leads to effective spatial separation of the majority of carriers, and hence, the value of γ is significantly lower than that obtained for pristine P3HT. In the BHJ sample, the high-frequency photoconductance signal is dominated by the electrons in PCBM domains not only at device-optimized PCBM loadings[35] but also at much lower PCBM loadings.[36] The similarities between the BHJ and the solution-cast P3HT/PCBM samples indicate that in the latter this is also the case.

We observe that not only the yield for charge generation, probed by the ΔG_{EOP}, but also the second-order decay component (rate constant γ) of the $\Delta G(t)$ dynamics in the P3HT/fullerene films is very similar to a deliberately blended sample; therefore, we can conclude that PCBM is also forming domains in the P3HT/PCBM samples and is not merely dispersing within the amorphous volume fraction of P3HT.

Table 1 also shows that the rate coefficient k is quite insensitive to the precise nature of the sample preparation or illumination geometry and, within error, no significant changes are seen. The only samples that appear to deviate from the behavior described above are the P3HT/C_{60} bilayers illuminated through the air–film interface, which exhibit elevated first-order rate coefficients compared to the other samples. In this case, carrier generation seems to proceed primarily via exciton dissociation at a defined polymer/fullerene interface (Figure 1b), since little or no mixing of the C_{60} into the P3HT is observed. The electrons therefore reside in a fullerene film, and not in fullerene domains as in the solution-cast samples and the carrier dynamics are short-lived, characteristic of the fullerene structural family, such as single-walled carbon nanotubes.[38,43] Annealing of the (w-P3HT)/C_{60} sample changes k to a value similar to the solution-cast samples, consistent with a mixed polymer–fullerene composite in which exciton dissociation at the bulk heterojunction dominates charge generation and electrons reside in fullerene domains mixed in the polymer.

3.5. Effective Loading Ratio of Graded P3HT/PCBM Bilayers. After having established the resemblance of solution-cast P3HT/PCBM samples to BHJs, in this section, we address the question of how much fullerene mixes into P3HT, or the effective loading ratio of PCBM in P3HT/PCBM samples. We carried out a comparison of the charge generation between P3HT:PCBM samples with different PCBM loadings and P3HT/PCBM films with different P3HT thicknesses, so that the P3HT-to-PCBM mass ratio is also tuned. Figure 7 shows

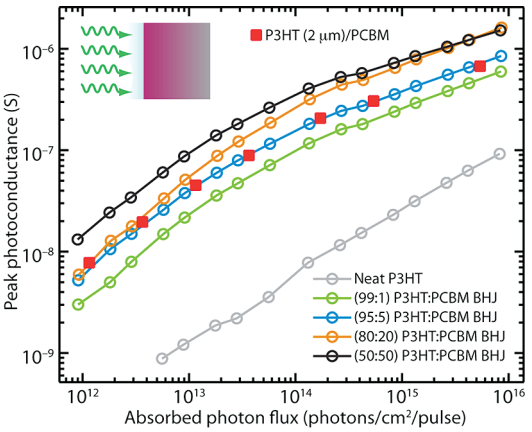

Figure 7. The peak (or end-of-pulse) photoconductance values as a function of absorbed photon flux for neat P3HT (gray circles); P3HT:PCBM blends with 1% (green circles), 5% (blue circles), 20% (orange circles), and 50% (black circles); and a sequentially deposited P3HT(2.4 μm)/PCBM sample in which the PCBM overlayer was solution-deposited (red squares). Note that the light intensity dependence of the peak photoconductance of the sequentially deposited sample overlaps with that of a blend with 5% PCBM loading. Illumination was performed through the substrate, as depicted in the cartoon, at a wavelength of 500 nm.

the peak photoconductance for a series of P3HT:PCBM BHJs with different PCBM loadings, ranging from 1 to 50% by weight. A solution-cast P3HT/PCBM sample with a 2.4 μm thick P3HT film is also shown for comparison. In this case, we conclude that this particular P3HT/PCBM sample has an effective loading of ca. 5% by weight of PCBM throughout the P3HT volume.

In order to relate the results presented here for thick ($d \approx 2.4$ μm) P3HT underlayers to the device data published previously,[15] we also investigated P3HT/PCBM samples in which the thickness of the polymer underlayer is varied from 75 nm to 2.4 μm and the PCBM overlayer is nominally 34 nm thick.[15] The result is shown in Figure 8, where the filled symbols (dots and squares) are the ΔG_{EOP} of P3HT/PCBM samples at a common absorbed photon flux of ~1 × 10^{12} photons/cm^2/pulse as a function of the underlayer P3HT thickness. For comparison, bands are also shown to indicate the $\Delta G_{EOP}/F_A$ ranges (mean ± standard deviation) at the same absorbed photon flux for P3HT:PCBM BHJs with PCBM loadings of 0 (neat-P3HT), 1, 5, 20, and 50%. A clear trend in the sequentially deposited samples can be observed: ΔG_{EOP} increases as the P3HT thickness decreases, which we attribute to a higher effective loading of PCBM resulting from the molecular diffusion process.[36] From Figure 8, the ΔG_{EOP} of a P3HT(75 nm)/PCBM has 5–20% by weight PCBM mixed into the polymer, P3HT(470 nm)/PCBM has ca. 5%, and the thick samples, P3HT(800 nm)/PCBM and P3HT(2.4 μm)/PCBM, have ca. 1–5% with the effective loading exceeding 5% in the annealed P3HT(2.4 μm)/PCBM sample.

We note that TRMC can only provide indirect evidence of the amount of PCBM in a mixed film, based on comparison of the magnitude of the photoconductance signal of sequentially deposited and intentionally mixed (BHJ) samples. Indeed, the errors associated with the estimates given above are quite large.

dx.doi.org/10.1021/jp212390p | J. Phys. Chem. C 2012, 116, 7293–7305

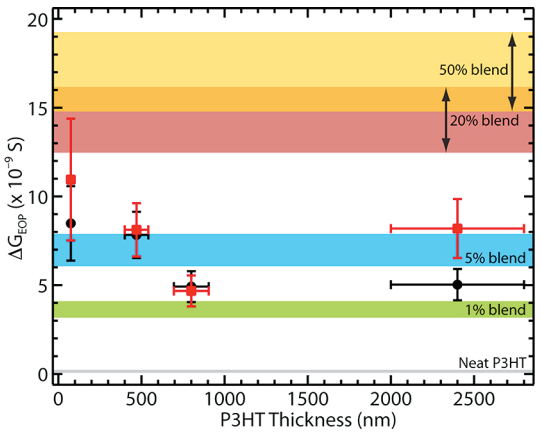

Figure 8. Photoconductance at a fixed photon flux of 1×10^{12} photons/cm^2/pulse for sequentially deposited samples with ~34 nm of PCBM on P3HT underlayers with different thicknesses: unannealed (black circles) and annealed (red squares). For comparison, the $\Delta G_{EOP}/F_A$ ranges for neat P3HT and P3HT:PCBM bulk heterojunctions with different PCBM loadings (1, 5, 20, and 50%) are also shown. Samples were illuminated at 500 nm through the quartz substrate.

However, the range of PCBM loadings we determine here for the P3HT(75 nm)/PCBM sample is consistent with the more accurate estimate provided for a sample of similar thickness by neutron reflectometry.[17] We also expect that the amount of PCBM that mixes into the P3HT underlayer will decrease with the use of doubly washed P3HT, as was used by Ayzner et al. in ref 15, as discussed above.

3.6. Comparison with P3HT/PCBM Bilayer Device Performance. The observations above go some way toward explaining the remarkable performance of OPV devices with a sequentially deposited P3HT/PCBM active layer:[15] during deposition of the PCBM overlayer, a mixed structure forms whose local conductivity resembles a BHJ. As a result, efficient exciton dissociation[15] and free carrier generation are observed (this work). We note, however, that the final process toward generating photocurrent in an OPV device, that of percolation of charge carriers to the electrodes, is not probed by a high frequency contactless technique such as TRMC.[34,44] Indeed, while a P3HT:PCBM BHJ film with only 1% by weight PCBM has a TRMC signal that is qualitatively very similar to the device-optimized 50% blend,[36] it would yield a short circuit current density that is almost the same as that of a pure P3HT device due to the absence of a percolation pathway for electrons. In the case of the sequentially deposited samples shown here, the insensitivity of TRMC to long-range percolation manifests itself in the insensitivity of the photoconductance of the solution-cast P3HT/PCBM sample to annealing (Figure 5 and Table 1). By contrast, annealing considerably improves the device performance as observed by Ayzner et al.[15]

This limitation of TRMC notwithstanding, we can still point out the somewhat surprising observation that the loading of PCBM in a sequentially deposited P3HT/PCBM sample seems to be lower than 20% by weight when P3HT is ca. 75 nm thick (Figure 8). This is significantly lower than the optimized 50% weight ratio in BHJ devices and warrants some discussion. The P3HT:PCBM BHJ is considered as somewhat of an oddity because the optimized blending ratio is 1:1 (or 50% PCBM) by weight, as opposed to many other polymer:PCBM BJHs where a higher loading of PCBM (up to 1:4) is required. It has been proposed that this occurs because the density of the hexyl side chains of P3HT prevents intercalation of the PCBM; therefore, PCBM is effectively "expelled" from crystalline P3HT domains, eliminating the need for excess PCBM to both fill available intercalation sites *and* form a percolation pathway for electrons.[45] However, there is a considerable volume of amorphous P3HT in a typical film,[46−49] and it is this disordered polymer phase into which the PCBM initially mixes.[18,50] It has been estimated that 40−50% of the volume of P3HT is amorphous;[48,49] therefore, the ratio of disordered P3HT to PCBM in an optimized BHJ (50% PCBM by weight) is between 1:2.5 and 1:2, which seems similar to other polymer:PCBM blends. With this simple observation in mind, we can now postulate that a PCBM loading as low as 20% by weight in the P3HT/PCBM sample studied here effectively equates to an approximately 2:1 P3HT:PCBM blend in the amorphous volume of P3HT, i.e., a much more reasonable blend ratio from a percolation standpoint.

That said, it is certainly plausible that when PCBM mixes into an already cast, solid P3HT film the resulting morphology is different than in a sample where the P3HT and PCBM are deposited concurrently from a mixed solution. Indeed, Gevaerts et al.[51] have argued that, even though PCBM intermixes with P3HT in sequentially processed films, the morphology of such films and thus their operation in the active layer of OPV devices is different from that of a conventional BHJ. On the basis of the arguments above, we believe that, in sequentially processed films, the PCBM may mix in to form a more optimal network than in BHJs that have higher fullerene loadings, where some PCBM is "wasted". Clearly, further structural studies are needed to precisely understand the differences and similarities between sequentially processed films and conventional BHJs.

4. CONCLUSIONS

With the TRMC technique, we have the ability to probe carriers in *sequentially* deposited layers of P3HT and fullerene where the P3HT/fullerene interface is created via either solution deposition or thermal evaporation. We conclude the following:

(I) Solution-deposited fullerene, namely, PCBM, always mixes with P3HT, including P3HT with thickness ranging from 75 nm up to 2.4 μm. This mixing is responsible for an increased photoconductance signal that resembles a BHJ sample.

(II) Removing part of the low-M_W fraction of P3HT by pretreating it with DCM, the solvent used to deposit the fullerene overlayer, hinders but does not completely inhibit fullerene diffusion into the P3HT underlayer, as evidenced by the magnitude and decay dynamics of the measured photoconductance.

(III) Thermal evaporation of a C_{60} overlayer on top of a P3HT underlayer does not result in extensive fullerene diffusion into the polymer. For excitation through the polymer, the photoconductance signal was similar in magnitude and shape to that of a neat-P3HT film, provided that the thickness of the P3HT is larger than the exciton diffusion length and that the sample had not been subjected to thermal annealing.

(IV) In all cases, thermal annealing causes intermixing of the polymer and fullerene components, for both solution-deposited PCBM and evaporation-deposited C_{60}.

dx.doi.org/10.1021/jp212390p | J. Phys. Chem. C 2012, 116, 7293−7305

(V) The magnitude of the photoconductance of solution-deposited P3HT/PCBM samples increased with the decreasing ratio of the nominal P3HT-to-fullerene thicknesses, consistent with the idea that mass action can drive more fullerene into thinner underlayers. The effective PCBM loading (by weight) in the intermixed phase could be controlled between about 2 and 20% depending on the P3HT underlayer thickness, consistent with previous work.[17]

(VI) Analysis of the transient decays reveals that the charge carrier generation yield and the dynamics of polymer/fullerene samples resemble that of a BHJ, implying that PCBM forms domains in the sequentially deposited P3HT/PCBM samples from solution. However, the sequentially deposited samples appear to have less total fullerene content and different device behavior from BHJs, suggesting that there are morphological subtleties in the P3HT/PCBM samples that cannot be discerned with the TRMC technique.

We note that the high sensitivity of TRMC to the carrier generation at a BHJ-like interface throughout the volume of the P3HT/PCBM films used here makes it unsuitable for the study of carrier generation by long-range energy transfer mechanisms[32] that may also be taking place as a consequence of the new morphological architecture. Therefore, the measurements reported here cannot rule out that such mechanisms occur in solution-processed P3HT/PCBM bilayers.

AUTHOR INFORMATION

Corresponding Author

*E-mail: nikos.kopidakis@nrel.gov.

Present Address

[§]Stanford Synchrotron Radiation Lightsource, 2575 Sandhill Road, MS:99, Menlo Park, CA 94025, United States.

Notes

The authors declare no competing financial interest.

ACKNOWLEDGMENTS

We thank Dr. David Coffey for the evaporation of C_{60} layers, Dr. Ziqi Liang for washing the P3HT in DCM, and Dr. Garry Rumbles for fruitful discussions. This work was supported as part of the Energy Frontier Research Center "Molecularly Engineered Energy Materials (MEEMs)" funded by the U.S. Department of Energy, Office of Science, Office of Basic Energy Sciences under Contract Number DE-SC0001342:001.

REFERENCES

(1) Green, M. A.; Emery, K.; Hishikawa, Y.; Warta, W. *Prog. Photovoltaics* **2011**, *19*, 84−92.

(2) Blom, P. W. M.; Mihailetchi, V. D.; Koster, L. J. A.; Markov, D. E. *Adv. Mater.* **2007**, *19*, 1551−1566.

(3) Thompson, B. C.; Frechet, J. M. J. *Angew. Chem., Int. Ed.* **2008**, *47*, 58−77.

(4) Brabec, C. J.; Gowrisanker, S.; Halls, J. J. M.; Laird, D.; Jia, S.; Williams, S. P. *Adv. Mater.* **2010**, *22*, 3839−3856.

(5) Kroeze, J. E.; Savenije, T. J.; Vermeulen, M. J. W.; Warman, J. M. *J. Phys. Chem. B* **2003**, *107*, 7696−7705.

(6) Lüer, L.; Egelhaaf, H.-J.; Oelkrug, D.; Cerullo, G.; Lanzani, G.; Huisman, B. H.; de Leeuw, D. *Org. Electron.* **2004**, *5*, 83−89.

(7) Goh, C.; Scully, S. R.; Mcgehee, M. D. *J. Appl. Phys.* **2007**, *101*, 114503.

(8) Shaw, P. E.; Ruseckas, A.; Samuel, I. D. W. *Adv. Mater.* **2008**, *20*, 3516−3520.

(9) Zhang, F. L.; Jespersen, K. G.; Björström, C.; Svensson, M.; Andersson, M. R.; Sundström, V.; Magnusson, K.; Moons, E.; Yartsev, A.; Inganäs, O. *Adv. Funct. Mater.* **2006**, *16*, 667−674.

(10) Li, G.; Yao, Y.; Yang, H.; Shrotriya, V.; Yang, G.; Yang, Y. *Adv. Funct. Mater.* **2007**, *17*, 1636−1644.

(11) Padinger, F.; Rittberger, R. S.; Sariciftci, N. S. *Adv. Funct. Mater.* **2003**, *13*, 85−88.

(12) Ma, W.; Yang, C.; Gong, X.; Lee, K.; Heeger, A. J. *Adv. Funct. Mater.* **2005**, *15*, 1617−1622.

(13) Peet, J.; Kim, J. Y.; Coates, N. E.; Ma, W. L.; Moses, D.; Heeger, A. J.; Bazan, G. C. *Nat. Mater.* **2007**, *6*, 497−500.

(14) Yao, Y.; Hou, J.; Xu, Z.; Li, G.; Yang, Y. *Adv. Funct. Mater.* **2008**, *18*, 1783−1789.

(15) Ayzner, A. L.; Tassone, C. J.; Tolbert, S. H.; Schwartz, B. J. *J. Phys. Chem. C* **2009**, *113*, 20050−20060.

(16) Reese, M. O.; White, M. S.; Rumbles, G.; Ginley, D. S.; Shaheen, S. E. *Appl. Phys. Lett.* **2008**, *92*, 053307.

(17) Lee, K. H.; Schwenn, P. E.; Smith, A. R. G.; Cavaye, H.; Shaw, P. E.; James, M.; Krueger, K. B.; Gentle, I. R.; Meredith, P.; Burn, P. L. *Adv. Mater.* **2011**, *23*, 766−770.

(18) Treat, N. D.; Brady, M. A.; Smith, G.; Toney, M. F.; Kramer, E. J.; Hawker, C. J.; Chabinyc, M. L. *Adv. Energy Mater.* **2010**, *1*, 82−89.

(19) Collins, B. A.; Gann, E.; Guignard, L.; He, X.; McNeill, C. R.; Ade, H. *J. Phys. Chem. Lett.* **2010**, *1*, 3160−3166.

(20) Drees, M.; Premaratne, K.; Graupner, W.; Heflin, J. R.; Davis, R. M.; Marciu, D.; Miller, M. *Appl. Phys. Lett.* **2002**, *81*, 4607−4609.

(21) Drees, M.; Davis, R. M.; Heflin, J. R. *Phys. Rev. B* **2004**, *69*, 165320.

(22) Drees, M.; Davis, R. M.; Heflin, J. R. *J. Appl. Phys.* **2005**, *97*, 036103.

(23) Geiser, A.; Fan, B.; Benmansour, H.; Castro, F.; Heier, J.; Keller, B.; Mayerhofer, K. E.; Nüesch, F.; Hany, R. *Sol. Energy Mater. Sol. Cells* **2008**, *92*, 464−473.

(24) Kaur, M.; Gopal, A.; Davis, R. M.; Heflin, J. R. *Sol. Energy Mater. Sol. Cells* **2009**, *93*, 1779−1784.

(25) Wang, D. H.; Lee, H. K.; Choi, D.-G.; Park, J. H.; Park, O. O. *Appl. Phys. Lett.* **2009**, *95*, 043505.

(26) Wang, D. H.; Choi, D.-G.; Lee, K.-J.; Im, S. H.; Park, O. O.; Park, J. H. *Org. Electron.* **2010**, *11*, 1376−1380.

(27) Wang, D. H.; Choi, D.-G.; Park, O. O.; Park, J. H. *J. Mater. Chem.* **2010**, *20*, 4910−4915.

(28) Dicker, G.; de Haas, M. P.; Siebbeles, L. D. A. *Phys. Rev. B* **2005**, *71*, 155204.

(29) Dicker, G.; de Haas, M. P.; Siebbeles, L. D. A.; Warman, J. M. *Phys. Rev. B* **2004**, *70*, 045203.

(30) Ferguson, A. J.; Kopidakis, N.; Shaheen, S. E.; Rumbles, G. *J. Phys. Chem. C* **2008**, *112*, 9865−9871.

(31) Lloyd, M. T.; Lim, Y.-F.; Malliaras, G. G. *Appl. Phys. Lett.* **2008**, *92*, 143308.

(32) Coffey, D. C.; Ferguson, A. J.; Kopidakis, N.; Rumbles, G. *ACS Nano* **2010**, *4*, 5437−5445.

(33) Savenije, T. J.; Kroeze, J. E.; Wienk, M. M.; Kroon, J. M.; Warman, J. M. *Phys. Rev. B* **2004**, *69*, 155205.

(34) Kroeze, J. E.; Savenije, T. J.; Warman, J. M. *J. Am. Chem. Soc.* **2004**, *126*, 7608−7618.

(35) Grzegorczyk, W. J.; Savenije, T. J.; Dykstra, T. E.; Piris, J.; Schins, J. M.; Siebbeles, L. D. A. *J. Phys. Chem. C* **2010**, *114*, 5182−5186.

(36) Ferguson, A. J.; Kopidakis, N.; Shaheen, S. E.; Rumbles, G. *J. Phys. Chem. C* **2011**, *115*, 23134−23148.

(37) O'Brien, D.; Weaver, M. S.; Lidzey, D. G.; Bradley, D. D. C. *Appl. Phys. Lett.* **1996**, *69*, 881−883.

(38) Holt, J. M.; Ferguson, A. J.; Kopidakis, N.; Larsen, B. A.; Bult, J.; Rumbles, G.; Blackburn, J. L. *Nano Lett.* **2010**, *10*, 4627−4633.

(39) Dicker, G.; de Haas, M. P.; Warman, J. M.; de Leeuw, D. M.; Siebbeles, L. D. A. *J. Phys. Chem. B* **2004**, *108*, 17818−17824.

(40) Chen, D.; Liu, F.; Wang, C.; Nakahara, A.; Russell, T. P. *Nano Lett.* **2011**, *11*, 2071−2078.

(41) Chen, L.-M.; Hong, Z.; Li, G.; Yang, Y. *Adv. Mater.* **2009**, *21*, 1434−1449.
(42) McMahon, D. P.; Cheung, D. L.; Troisi, A. *J. Phys. Chem. Lett.* **2011**, *2*, 2737−2741.
(43) Ferguson, A. J.; Blackburn, J. L.; Holt, J. M.; Kopidakis, N.; Tenent, R. C.; Barnes, T. M.; Heben, M. J.; Rumbles, G. *J. Phys. Chem. Lett.* **2010**, *1*, 2406−2411.
(44) Rance, W. L.; Ferguson, A. J.; McCarthy-Ward, T.; Heeney, M.; Ginley, D. S.; Olson, D. C.; Rumbles, G.; Kopidakis, N. *ACS Nano* **2011**, *5*, 5635−5646.
(45) Mayer, A. C.; Toney, M. F.; Scully, S. R.; Rivnay, J.; Brabec, C. J.; Scharber, M.; Koppe, M.; Heeney, M.; McCulloch, I.; McGehee, M. D. *Adv. Funct. Mater.* **2009**, *19*, 1173−1179.
(46) Brinkmann, M.; Rannou, P. *Adv. Funct. Mater.* **2007**, *17*, 101−108.
(47) Moulé, A. J.; Meerholz, K. *Adv. Funct. Mater.* **2009**, *19*, 3028−3036.
(48) Clark, J.; Chang, J.-F.; Spano, F. C.; Friend, R. H.; Silva, C. *Appl. Phys. Lett.* **2009**, *94*, 163306.
(49) Reid, O. G.; Nekuda-Malik, J. A.; Latini, G.; Dayal, S.; Kopidakis, N.; Silva, C.; Stingelin, N.; Rumbles, G. *J. Polym. Sci., Part B: Polym. Phys.* **2012**, *50*, 27−37.
(50) Yin, W.; Dadmun, M. *ACS Nano* **2011**, *5*, 4756−4768.
(51) Gevaerts, V. S.; Koster, L. J. A.; Wienk, M. M.; Janssen, R. A. J. *ACS Appl. Mater. Interfaces* **2011**, *3*, 3252−3255.